Green Synthesis of Zinc Oxide Nanoparticles Using *Centella asiatica* (L.) Urb. Extract: Characteristics and Applications

Kim Ngan Thi Tran[1*], Khanh Van Tran Le[1], Cat Thuyen Ngoc Vo[2], Cat Nguyen Ngoc Vo[2], Danh Hoang Pham[1], and Tuu Thi Tran[1]

[1]*Institute of Applied Technology and Sustainable Development, Nguyen Tat Thanh University, Ho Chi Minh City 700000, Vietnam*

[2]*Faculty of Chemical Engineering and Food Technology, Nong Lam University, Ho Chi Minh City 700000, Vietnam*

* ***Corresponding author:***

email: nganttk@ntt.edu.vn

Received: November 7, 2024
Accepted: May 2, 2025

DOI: 10.22146/ijc.101359

Abstract: Centella asiatica *is one of the popular plant sources used in green synthesis application due to its antibacterial and cell regeneration stimulating properties. The objective of studying the synthesis process of ZnO nanoparticles in pennywort extract is to analyze the structure and morphology of materials using modern analytical methods. ZnO nanoparticles are used to remove CIP antibiotics in wastewater and are intended for application in cosmetic products. The results of the adsorption process to remove the antibiotic ciprofloxacin after 90 min, with an adsorption dose of 0.005 g* L^{-1}*, an initial concentration of 100 mg* L^{-1} *in a pH 6 environment, showed an adsorption capacity of 152.93 mg* g^{-1}*. The adsorption data followed the pseudo-second-order adsorption kinetic model and the Dubinin-Radushkevich adsorption isotherm model according to the non-linear regression method. The synthetic ZnO nanoparticles in a skincare mask product application with an SPF index of 14.12 and sun protection ability of 93.92% were evaluated.*

Keywords: *zinc oxide nanoparticles; adsorption; cosmetic; green synthesis; kinetics; isotherms*

■ INTRODUCTION

Zinc oxide (ZnO) nanoparticles are composed of zinc (Zn) and oxygen (O) atoms arranged in a crystal lattice structure. They are often synthesized through various methods, including sol-gel synthesis, precipitation and hydrothermal methods [1-3]. ZnO nanoparticles are typically 1 to 100 nm in size, with unique properties depending on size and morphology [4]. Due to their small size, ZnO nanoparticles have a high surface area to volume ratio, which enhances reactivity and makes them suitable for various applications. Additionally, ZnO nanoparticles synthesized from plant extracts are an environmentally friendly and sustainable method of nanoparticle production compared to traditional chemical methods [5–7]. Green synthesis using plant extracts involves phytochemicals such as flavonoids, phenolics, terpenoids, and alkaloids chosen for their reducing and stabilizing properties [8-11]. Common sources include green tea, pennywort, neem leaves, aloe vera, and fruit peels, which are inexpensive ingredients that are naturally available and easy to use for large-scale extraction and synthesis [8,12-15]. For example, orange peel extract was used as a reducing agent in the synthesis of ZnO particles from zinc acetate dihydrate, demonstrating effective antibacterial ability against *Staphylococcus aureus* and *Escherichia coli* strains [16]. Furthermore, ZnO particles with a hexagonal wurtzite structure with sizes in the range of 7–11 nm synthesized from Gotukola extract exhibited strong antioxidant ability through scavenging DPPH free radicals [17]. In addition, the leaf extract of *Syzygium cumini* is used to synthesize ZnO nanoparticles for the application of removing 91.4% of methylene blue pigment in textile wastewater [18].

Pennywort (*Centella asiatica* (L.) Urb.), belonging to the Apiaceae family, is a herb that grows wild and widely distributed in many warm and rainy areas around the world, especially in tropical areas in Asia and other tropical regions [19-20]. Pennywort is suitable for

tropical or subtropical climates with high temperatures and humidity, and it has the ability to adapt to many different soil types and environments [21-22]. It is commonly used for nutritional and medicinal purposes in its distribution areas. Pennywort has many identifying characteristics. Pennywort leaves are often round or heart-shaped with bright green leaf patches. Pennywort has a long, soft stem that emerges from the base of the plant. The flowers of pennywort have a special shape, consisting of many small petals and sepals. Pennywort has a characteristic mild and aromatic flavor, often described as moist, earthy, and mildly herbal. Pennywort is rich in bioactive compounds such as triterpenoid saponins, flavonoids, and polyphenols [12,14], that can act as reducing and stabilizing agents in the synthesis of ZnO nanoparticles.

Nanoparticles synthesized from *C. asiatica* exhibit excellent UV-blocking properties, making them ideal candidates for sun care products such as sunscreens and lotions, which can provide broad-spectrum UV protection and enhance the photostability of cosmetic formulations. Additionally, synthesized ZnO nanoparticles can be used in water treatment systems to remove antibiotics from contaminated water sources. This application is especially important given growing concerns about antibiotic pollution and its impact on aquatic ecosystems and human health. Therefore, the purpose of this study is to create ZnO nanoparticles using a green method based on pennywort extract. The synthesized ZnO nanoparticles can then be used in water treatment systems to remove antibiotics from contaminated water sources. Furthermore, the synthesized ZnO particles are intended for integration into cosmetic products to provide broad-spectrum UV protection and enhance the photostability of cosmetic formulations (Fig. 1).

■ EXPERIMENTAL SECTION

Materials

Chemical synthesis of materials in this study includes: zinc nitrate hexahydrate ($Zn(NO_3)_2{\cdot}6H_2O$, 99%), sodium hydroxide (NaOH, 99%), ethanol (C_2H_5OH, 99.7%) obtained from Xilong Chemical Co., Ltd. (Shantou, China). Ciprofloxacin (CIP, $C_{18}H_{20}FN_3O_4$), 2,2-diphenyl-1-picrylhydrazyl (DPPH, $C_{18}H_{12}N_5O_6$), Folin Ciocalteu's phenol reagent was purchased from Sigma-Aldrich Co. (St. Louis, MO, USA). Cosmetic chemicals: non-ionic surfactants, emollients, moisturizers, preservatives, were purchased at Nguyen Ba Trading Production Co., Ltd, Tan Binh District, HCMC, Vietnam.

Pennywort was purchased at gardeners in the Mekong Delta and transported to the laboratory. The ingredients were rinsed to remove dirt, impurities and residual chemicals on the surface. Then, pennywort was dried at 50 °C before extraction to reduce decomposition or mold growth during storage.

Instrumentation

Some of the equipment used in the study includes an Agilent Cary 60 UV-vis spectrophotometer (USA), pH value was measured by a Hanna HI2210-02 benchtop pH meter (Romania), MB90 Ohaus moisture balance (USA), 4-position digital heating magnetic stirrer MS-H340-S4 DLAB, China, Ybotech Tg16/Tgl16 high-speed benchtop centrifuge, China, Memmert UN110 drying oven, Germany. All equipment operated stably.

Procedure

Extraction process of pennywort plant

Dried pennywort was ground into a fine powder. The extract was prepared by taking 1 g of leaf powder mixed with 100 mL of three solvents: ethanol, water, and ethanol:water (1:1) and heated at 60 °C for 90 min. The resulting extract was filtered with Whatman No. 1 filter paper, cooled to ambient temperature, and stored at 4 °C for later use. The extract with the highest biological activity was selected to synthesize ZnO materials.

Preliminary research on botanical chemistry

Polyphenol content was determined based on samples complexed with Folin-Ciocalteu's alkaline solution according to Pham et al. [23] adjusted method. The reaction mixture included 0.5 mL of sample solution and 2.5 mL of 10% Folin-Ciocalteu reagent, shaken well with a Vortex machine, and allowed to react

for 5 min. Then, 2.0 mL of 7.5% Na_2CO_3 solution was added, and the solution was left in the dark for 1 h at room temperature. The absorbance of the mixture was measured spectrophotometrically at 765 nm.

DPPH scavenging activity was determined based on the DPPH free radical scavenging method based on the publication of Pham et al. [23] with modifications. The absorption of the solution was analyzed on a UV-vis spectrophotometer at 517 nm. The stock DPPH solution was made by weighing 0.012 g of DPPH, adding enough 50 mL of ethanol, shaking well and stabilizing in the dark at 4 °C. An amount of stock solution (10 mL) was added to 45 mL of ethanol, corrected to an absorbance value of 1.10 ± 0.02. Samples were prepared with 0.5 and 1.5 mL of DPPH added to the test tube and shaken well on a Vortex machine. After incubation for 30 min in the dark, the solution was measured for absorbance based on the ascorbic acid standard curve.

Synthesis of ZnO materials from vegetable extracts

The synthesis process of ZnO nanoparticles, including Zinc nitrate hexahydrate and pennywort extract, was simulated according to the publication of Jayachandran et al. [12] with modifications, 10 mL of pennywort extract was added to 100 mL of 0.1 M $Zn(NO_3)_2$ while continuously stirring. After 2 h, 1 mL of 1 M NaOH solution was added to the mixture to form a precipitate, and the mixture was stirred for another 1 h. The precipitate was recovered by centrifugation at 6000 rpm for 10 min and washed with ethanol to remove impurities. The mixture was then dried overnight at 120 °C to obtain a light blue powder. The resulting powder was ground to achieve a consistent powder, and heat treatment was continued at 500 °C for 2 h to produce white ZnO nanoparticle. The final sample was stored in a glass-closed vial and used for characteristic analysis.

Structural characteristics of ZnO

The crystal structure of the material was determined by X-ray diffraction (XRD) method (D8 Advanced – Hitachi – Germany), with Cu-Kα = 1.5406 Å as the radiation source and scanning angle 2θ varying from 10–70°. The proportion of elements on the surface of the material and the detection of any other elements that may be present due to impurities were determined using energy dispersive X-ray (EDX) spectroscopy. The morphology, surface structure and size distribution of ZnO particles were analyzed based on SEM analysis method (S4800 - JEOL Japan). Information about the chemical composition, molecular structure and bonding characteristics of the material based on the interaction with infrared light was determined on a Nicolet 6700 device (Thermo Fisher Scientific, USA). BET analysis of ZnO provides important quantitative data on the surface

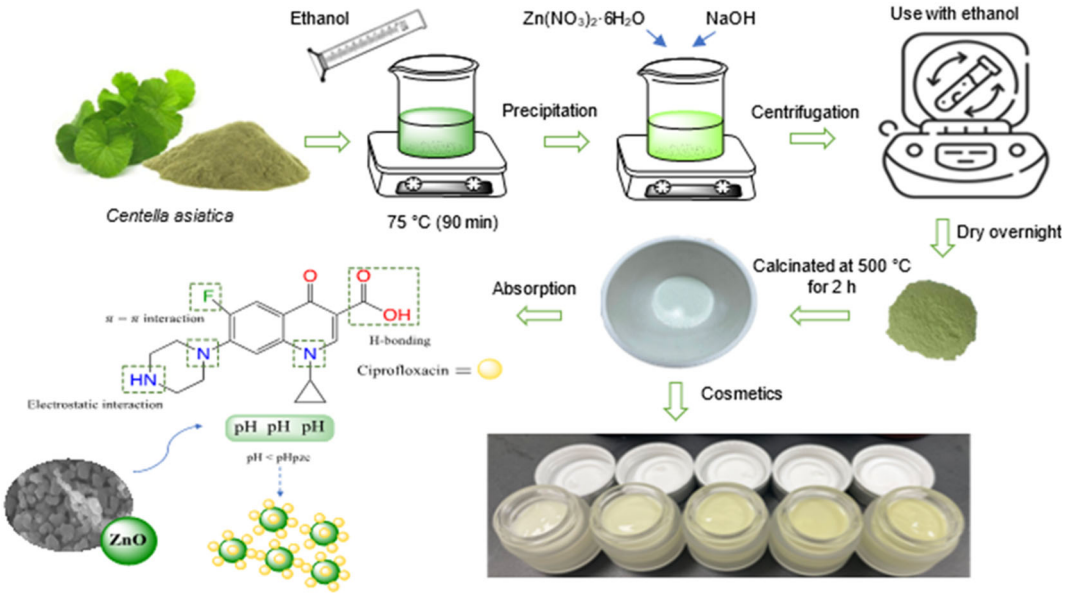

Fig 1. Research scheme on the synthesis of ZnO nanoparticles and their applications

area, porosity and shape of the adsorption and desorption isotherms. The hysteresis loop in BET analysis reveals information about the pore structure by Micromeritics 2020 - Micromeritics (USA).

Adsorption activity of the CIP antibiotic by ZnO

First, the CIP solution is standardized to a certain concentration suitable for creating experimental conditions. The antibiotic solution is completely dissolved under the influence of an ultrasonic bath and the control solution concentration is measured at a wavelength of 273 nm. An amount of ZnO material and add it to a 250 mL Erlenmeyer flask with 50 mL CIP, placed on a thermostatic shaker (Jeotech – Korea). The influencing conditions are specifically investigated, such as CIP antibiotics prepared with a concentration range of 20 to 150 mg L^{-1}, material dosage (0.002 to 0.04 g L^{-1}), pH is adjusted from 2 to 10, the process takes place continuously for a specified time from 10 to 210 min to achieve adsorption equilibrium. After that, the ZnO material is separated from the solution at 6000 rpm for 10 min, the remaining CIP solution is analyzed by UV spectroscopy at 273 nm to determine the adsorption ability of ZnO material for CIP.

Formula of cream skin care mask product

The ingredients are included in the formula in different concentrations, and the appropriate amounts are chosen to add to the formula (Table 1). Kaolin powder is soft and smooth, helping to absorb sebum, soothe acne and irritated skin. Additional additives such as softeners, antioxidants, and surfactants are mixed based on their function and the amount of influence in the formula. The oil phase components (extract, cetyl alcohol, salicylic acid) are weighed, mixed, and stirred continuously with a mechanical stirrer at 80 °C to form a homogeneous liquid. Similarly, the components of the water phase are weighed, mixed and stirred continuously with a mechanical stirrer at 80 °C. The phases are mixed by continuous stirring for 30 min until a uniform distribution of the components is achieved. Scents and colors are added to increase the aesthetics of the product. All samples are stable for 24 h at room temperature.

Sun protection factor (SPF) analysis

The process of determining the SPF index requires care and precision to ensure sunscreen products meet safety standards and are effective in protecting the skin from the harmful effects of UV rays. According to the Mansur et al. [24], the volume of 0.2 g of each cream mask product formulation was diluted with ethanol solvent and titrated to 100 mL. The absorbance of the analyzed product on the photometer was measured at wavelengths of about 290–320 nm (UVB radiation range) at each 5 nm distance. The Mansur equation (Eq. (1)) is applied to calculate the SPF index;

$$SPF = CF\sum_{290}^{320} EE(\lambda)\times 1(\lambda)\times Abs \quad (1)$$

where Abs (λ) is the value of spectral absorbance at wavelength λ, CF is the correction factor (10), EE (λ) × 1 is the red blood cell effect of radiation with wavelength λ. The values of EE x λ are constant.

Table 1. Formula ingredients of skin care mask products

Ingredients	Formulation (%)					
	F0	F1	F2	F3	F4	F5
Kaolin	5.50	5.50	5.50	5.50	5.50	5.50
Cetyl alcohol	4.00	4.00	4.00	4.00	4.00	4.00
Coco glucoside	2.75	2.75	2.75	2.75	2.75	2.75
Salicylic acid	0.50	0.50	0.50	0.50	0.50	0.50
Glycerin	1.00	1.00	1.00	1.00	1.00	1.00
Pennywort extract	0.00	0.50	2.50	5.00	7.50	10.00
Citric acid	0.75	0.75	0.75	0.75	0.75	0.75
ZnO	0.10	0.10	0.10	0.10	0.10	0.10
Tea tree essential oil	0.50	0.50	0.50	0.50	0.50	0.50
Water, qs, 100	qs	qs	qs	qs	qs	qs

■ RESULTS AND DISCUSSION

Preliminary Physicochemical Activity of Pennywort Extract

Polyphenol, DPPH, and vitamin C tests were conducted through testing procedures. From Table 2, it can be inferred that the solvent EtOH is more dominant than the remaining solvents, which will be reflected in the analysis of TPC and DPPH. With high polyphenol content in the alcohol extract, polyphenols extracted from pennywort can act as a green, sustainable reducing agent and stabilizer for the synthesis of ZnO nanoparticles. This approach eliminates the need for harmful chemicals and energy-intensive processes, making it environmentally friendly. Polyphenols act as stabilizers, enhancing the stability and dispersion of ZnO particles. ZnO nanoparticles synthesized with pennywort polyphenols have excellent UV–blocking properties, making them suitable for sunscreen formulations and UV-protective coatings [25-27].

Characteristics of ZnO Nanoparticle Structure

The XRD pattern of synthesized ZnO clearly shows the crystal structure of the synthesized nanoparticles (Fig. 2). Sharp diffraction peaks were observed at 2θ values of 31.74°, 34.41°, 36.22°, 47.53°, 56.59°, 62.87°, 66.39°, 67.96° and 69.06°. These peaks are indexed as the diffraction lattice planes of (100), (002), (101), (102), (110), (003), (200), (112), and (201), confirming the hexagonal wurtzite structure for nanoparticle synthesis. The data analysis results of the ZnO sample are similar to the standard spectrum ICSD 65119 in the "Cambridge Crystallographic Data Center (CCDC)". All peaks of ZnO nanoparticles are in good agreement with the standard diffraction pattern of the hexagonal-wurtzite crystal structure. The sharp and well-defined peaks indicate the crystalline nature of the synthesized ZnO nanoparticles. Phytochemical components in pennywort extract connect to the zinc surface in zinc nitrate to stimulate the creation of ZnO nanoparticles. Finally, under calcination temperature at ~500 °C, the mass of Zn nanoparticles is oxidized and produces crystalline ZnO nanoparticles. The Debye-Scherrer equation (Eq. (2)) relates the scattering of value 0.9, β is the full-width half-maximum (FWHM), λ is the wavelength of the X-ray (1.5406 Å), and θ is the corresponding Bragg's angle.

$$D = \frac{k\lambda}{\beta \cos\theta} \quad (2)$$

Calculating the size of ZnO nanoparticles from XRD data, the average crystalline size of ZnO nanoparticles is shown specifically in Table 3, indicating that ZnO nanoparticles have an average size of 27.6 nm. The results are similar to some previous publications, such as Gupta et al. [28] who synthesized ZnO nanoparticles from *Catharanthus roseus* (*C. roseus*) leaves with an average particle size of 36.83 nm. Additionally, ZnO nanoparticles with an average size of 31.1 nm were synthesized using zinc sulfate and pennywort extract [11].

The functional groups formed on the zinc oxide nanoparticle sample were examined using FTIR spectroscopy, as shown in Fig. 3. It is clear that the functional groups of zinc oxide nanoparticles from the

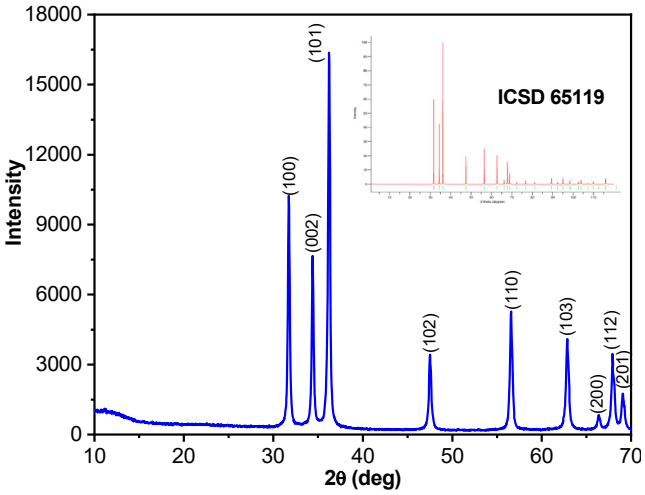

Fig 2. XRD profile of ZnO nanoparticle

Table 2. Phytochemistry of pennywort extract

	Water	Ethanol	Water:Ethanol
DPPH (mg/100 g DW)	256.706 ± 1.526	261.682 ± 4.311	253.199 ± 0.512
TPC (mgAAE/g 100 g DW)	450.952 ± 0.022	1567.773 ± 0.126	330.973 ± 0.034

Table 3. XRD analysis of ZnO nanoparticle size according to Scherrer equation

Peak position (2θ)	FWHM (β)	Miller indices	Particle size (nm)
31.73603	0.27725	(100)	29.7774188
34.40209	0.2877	(002)	28.8947214
36.22653	0.29658	(101)	28.1719928
47.53342	0.32189	(102)	26.9566067
56.59102	0.34376	(110)	26.2357817
62.8764	0.38758	(103)	24.0144148
66.38859	0.26952	(200)	35.2097888
67.96214	0.40095	(112)	23.884969
69.09029	0.37805	(201)	25.5022375

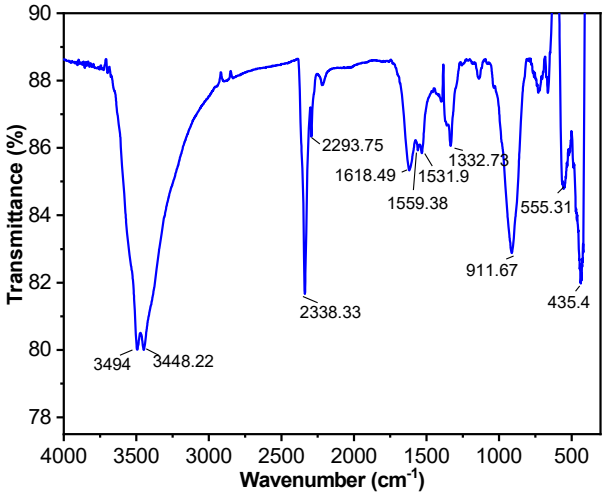

Fig 3. FTIR spectrum of ZnO nanoparticles

synthesis results in this study show a similar result to the previous study. FTIR analysis of ZnO was performed in the wavenumber range from 400 to 4000 cm^{-1}. The broad absorption peak at 3448 and 3494 cm^{-1} shows the stretching vibration of the O–H group [29]. Symmetric and asymmetric C–H group bonds at 2800–2900 cm^{-1} determine the negligible existence of intermediate products during synthesis or from processing and storage after synthesis [30]. The absorption peaks at 2338 and 2294 cm^{-1} were assigned to the CO_2 group. The absorption peak at 1627 cm^{-1} is attributed to C=C relaxation in the aromatic ring and C=O relaxation in polyphenols. At low wavenumbers, Zn–O groups were formed at 345 and 555 cm^{-1} [31-32]. These results showed that the ZnO particles were well configured as presented in the X-ray diffraction data. In addition, the Zn–OH group also appeared at approximately 600 and 912 cm^{-1} [33].

SEM images of ZnO nanoparticles synthesized using *C. asiatica* as a green synthesis method can reveal the size distribution and shape details of ZnO nanoparticles (Fig. 4(a)). Most of the particles are spherical and discrete, the particles form clearly and quite

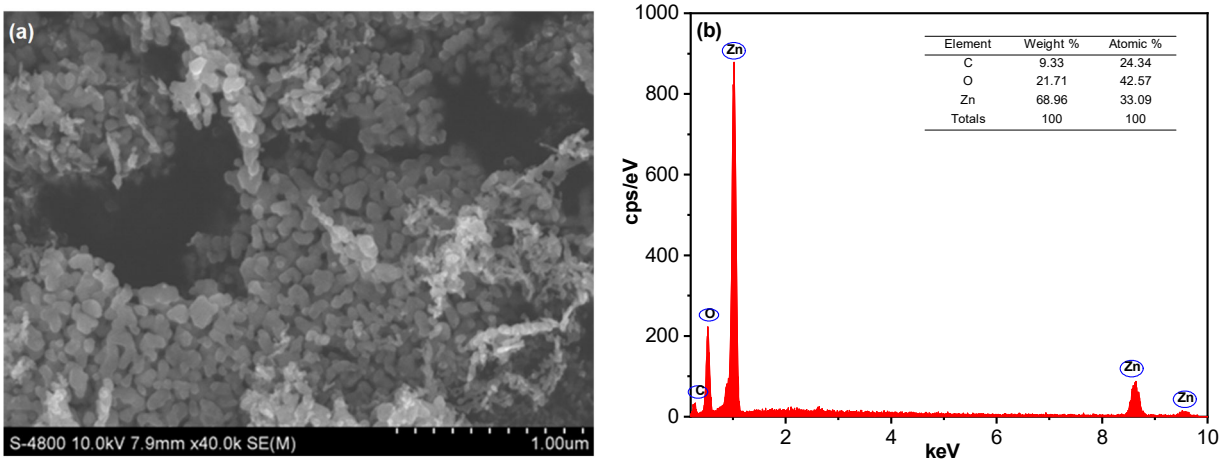

Fig 4. (a) SEM and (b) EDX profiles of ZnO nanoparticles

uniformly when heated at 500 °C. Through EDX spectrum analysis of ZnO, it is possible to evaluate the elemental fraction of the sample and draw conclusions about the chemical properties and structure of ZnO (Fig. 4(b)). This spectrum shows peaks that reflect the presence of elements in the sample mainly Zn and O, along with other elements that may be present due to impurities or other components. Typically, a significant carbon (C) peak is observed at about 0.2–0.3 keV in the EDX spectrum of ZnO material, indicating a carbon content of about 9%, indicating carbon impurities on ZnO nanoparticles. The Zn peak will appear in the spectrum at the energy characteristic of zinc around 1.0 and 8.6 keV. This peak confirms the presence of zinc in the nanoparticles and is predicted to be present in ZnO. Similarly, the oxygen peak will be observed at an oxygen-specific energy level of about 0.5 keV. This peak shows the presence of oxygen atoms in ZnO nanoparticles.

The BET surface area of the ZnO material was analyzed at a temperature of 77 K based on N_2 adsorption-desorption measurements. As shown in Fig. 5(a) and 5(b), based on the IUPAC classification, ZnO has a typical type IV isotherm with a hysteresis loop H3, implying a mesoporous crystalline material. This indicates the presence of mesopores (pores typically 2 to 50 nm in diameter). Using data obtained from the nitrogen adsorption-desorption isotherm and based on the slope and intercept of the BET plot of ZnO, the specific surface area was calculated to be 37.75 $m^2 g^{-1}$ and the pore size was 36.93 nm. Similarly, Khan and colleagues synthesized ZnO nanoparticles from passion fruit peel (*Passiflora incarnata* L.) with a BET surface area of 30.82 $m^2 g^{-1}$ [34]. In 2022, Su et al. [35] used the hydrothermal method to synthesize wurtzite hexagonal ZnO nanoparticles with different morphologies. The BET surface area of ZnO samples is in the order: nanorods (2.86 $m^2 g^{-1}$) < nanowires (4.32 $m^2 g^{-1}$) < nanospheres (6.47 $m^2 g^{-1}$) < nanoflakes (8.31 $m^2 g^{-1}$). The obtained BET surface area value reflects the accessible surface area of ZnO nanoparticles synthesized by the green method. This value can be compared with that of ZnO materials prepared by conventional methods to evaluate the effectiveness of green synthesis. Green synthesis methods utilize biological agents (such as plant extracts and microorganisms) instead of harsh chemicals. The synthesis process typically occurs at low temperatures and does not involve the use of toxic solvents. The BET surface area is generally large, depending on the material used. Green synthesis increases the number of adsorption sites and enhances the CIP adsorption capacity due to the rich pore surface and more porous structure, allowing for faster diffusion. In contrast, hydrothermal/conventional methods involve the use of organic solvents, metal salts, and chemical reducing agents. These methods require high temperatures (>100 °C) for an extended period. The lower BET surface area in these methods reduces the contact area of the material with the solution, limiting the CIP adsorption capacity due to the less porous surface. While these methods can create a homogeneous crystal structure, it is typically less porous [36].

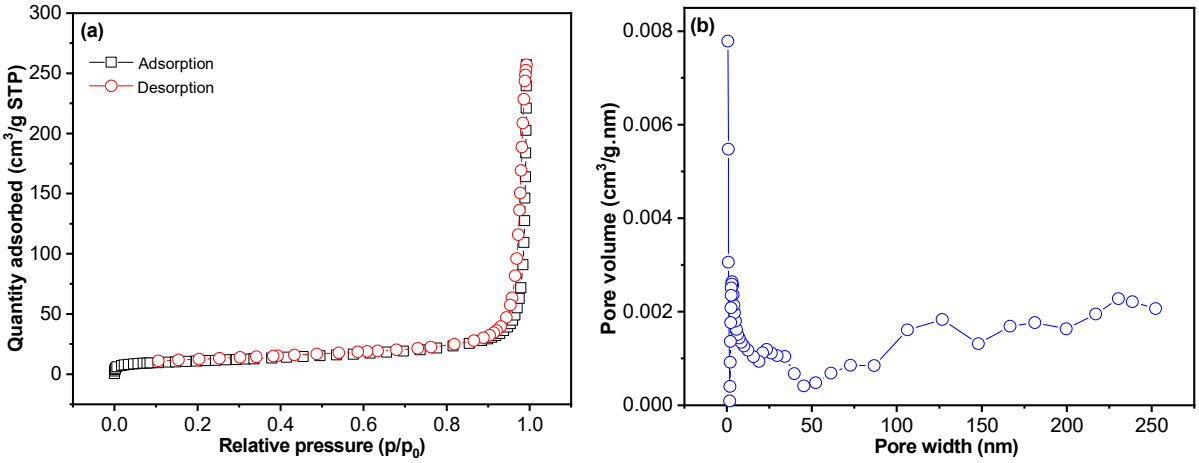

Fig 5. N_2 adsorption-desorption isotherm curve and pore size distribution of ZnO nanoparticles

CIP Antibiotic Adsorption Capacity of ZnO Material

Adsorption kinetics

Different kinetic models, such as pseudo-first-order (PFO), pseudo-second-order (PSO), Bangham, and Elovich, are used to study the kinetics of the adsorption process. The parameters and results of the kinetic models are listed in Table 4. The impact time is the time when CIP comes into contact with the ZnO adsorbent material and is also the time when the kinetic process takes place (Fig. 6(a)). This time can significantly affect the adsorption capacity of the material for CIP. Normally, as the impact time increases, the adsorption will gradually increase until it reaches a saturation level. ZnO was tested for its adsorption capacity by varying the oscillation time. Samples were taken at 10, 30, 60, 90, 120, 150, and 210 min respectively, to show the removal efficiency of CIP according to the built standard curve. As shown in Fig. 6(a), the adsorption capacity reached 86.5 mg g^{-1} after 90 min and reached the saturation level. The CIP concentration in the solution will not change significantly anymore. The CIP adsorption curve of ZnO nanoparticles shows the correlation coefficient R^2 as PSO > Elovich > Bangham > PFO, according to the PSO adsorption kinetic equation with the reliability coefficient R^2 = 0.9895, proving the adsorption rate is resistant. CIP production can be largely controlled by a chemical adsorption process through the ion exchange mechanism between the adsorbate and adsorbent by

Table 4. Parameters of non-linear kinetics for CIP adsorption on ZnO nanoparticles.

Kinetic models	Equation	Parameters	Value
Pseudo-first-order	$q_t = q_1\left(1-\exp\left(-k_1 t\right)\right)$	q_1 (mg g^{-1})	84.924
		k_1 (min^{-1}/(mg $L^{-1})^{1/n}$)	0.0618
		R^2	0.9624
Pseudo-second-order	$q_t = \dfrac{t}{\dfrac{1}{k_2 q_2^2}+\dfrac{t}{q_2}}$	1_2 (mg g^{-1})	93.404
		k_2 (g (mg min)$^{-1}$)	$9.629.10^{-4}$
		R^2	0.9895
Bangham	$\log\left(\dfrac{C_m}{C_m - q_t \cdot \dfrac{m}{V}}\right) = \log\left(\dfrac{k_B}{2.303 \cdot V}\right) + \alpha_B \log(t)$	k_B (mL (g $L^{-1})^{-1}$)	32.911
		α_B	0.1967
		R^2	0.9788
Elovich	$q_t = \dfrac{1}{\beta}\ln\alpha\beta + \dfrac{1}{\beta}\ln t$	α (mg (g min)$^{-1}$)	40.484
		β (g mg^{-1})	0.0883
		R^2	0.9889

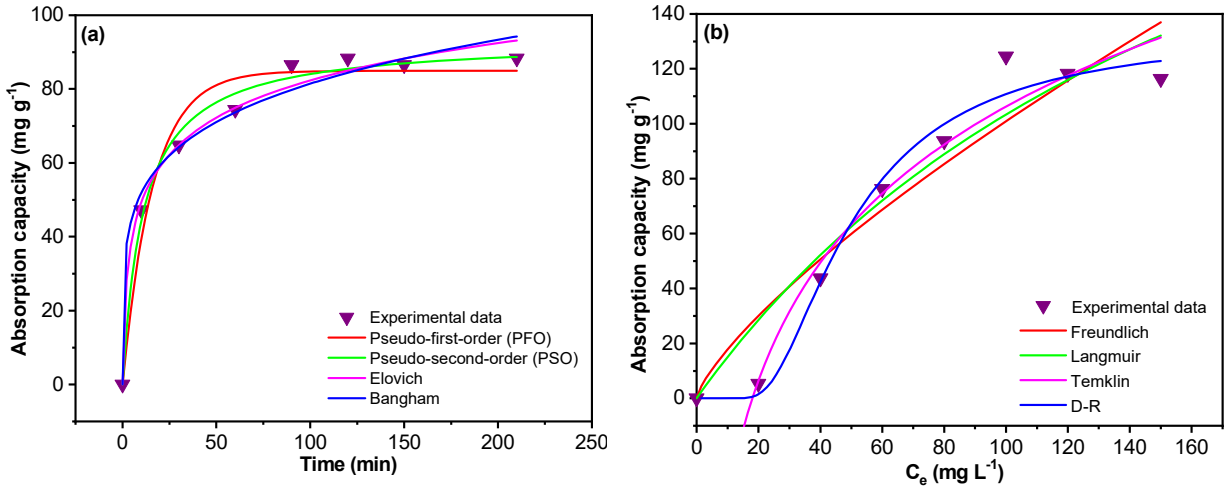

Fig 6. Non-linear fitting plots of (a) kinetics and (b) isotherms models CIP adsorption onto ZnO nanoparticles

chemical adsorption bonds. Additionally, the equilibrium adsorption capacity values calculated from the PSO equations are closer to the experimental values than the PFO equation. Therefore, it can be concluded that the apparent second-order kinetic equation is suitable for the CIP adsorption process of ZnO material. At the same time, based on the Elovich model experimental data, the values of the parameters α and β can be determined. These parameters provide detailed information about the adsorption rate and desorption constant of CIP on ZnO nanoparticles, which are 40.484 mg (g min)$^{-1}$ and 0.0883 g mg^{-1}, respectively, indicating that the adsorption process is more dominant than desorption, which is an indication of the efficiency and stability of the adsorption process.

Adsorption isotherms

Adsorption isotherm analysis plays a very important role in experimental design and the fabrication of adsorbent materials. Adsorption isotherms are tools that describe the relationship between the concentration of an adsorbate in the liquid phase and the concentration of the adsorbate on the surface of the adsorbent under specific conditions. Experimental data are analyzed using the Langmuir, Freundlich, Temkin and Dubinin-Radushkevich (D-R) isotherm models. Fig. 6(b) shows that increasing the initial CIP concentration from 20 to 150 mg L^{-1} decreased the CIP removal capacity from 124.53 to 116.43 at pH 6, an adsorption dose of 0.005 g L^{-1} and contact time of 90 min. Consistent with this result, Yousefi et al. reported that increasing the CIP concentration from 30 to 100 mg L^{-1} decreased the CIP removal efficiency from 83 to 59% [37]. In the study by Wang et al., the adsorption capacity of the adsorbent for cationic CIP increased rapidly for initial CIP concentrations below 50 mg L^{-1} and then decreased with increasing CIP initial concentrations above 50 mg L^{-1} [38]. This may be due to the lack of available sites on the adsorbent to adsorb high concentrations of CIP [39].

As the antibiotic concentration increases, surface saturation of ZnO can also be achieved faster. Surface saturation occurs when antibiotics have saturated the adsorption sites on the ZnO surface and are no longer capable of further adsorption. Antibiotic concentration can influence the chemical interactions between ZnO and antibiotics. CIP may interact with the surface at low concentrations mainly through weak bonds such as van der Waals forces or electrostatic interactions. As the CIP concentration increases, the distance between CIP molecules in the solution decreases, which may result in interactions between CIP molecules (hydrogen bonds or tighter packing on the adsorbent surface). These interactions may increase the overall affinity between CIP and the adsorbent but do not necessarily increase the adsorption capacity because the available sites are limited. However, if the surface is close to saturation, CIP may be adsorbed by a multilayer (Freundlich) mechanism or stronger interactions between CIP molecules (possibly clustering), which maintains removal efficiency but does not significantly increase q_e. Experimental data of the adsorption isotherm are shown in Fig. 6(b) and Table 5. The results indicate that the D-R (R^2 = 0.9783) and Temkin (R^2 = 0.9618) models are suitable to describe the adsorption process compared with the Langmuir (R^2 = 0.9175) and Freundlich (R^2 = 0.8894) models when using the non-linear isotherm equation. Adsorption of CIP onto ZnO nanomaterials occurs under heterogeneous surface conditions, in which the size and shape of the pores are variable. The D-R model fit suggests that adsorption may not be a purely homogeneous surface process but may involve capillaries or ion complex formation on the ZnO surface. The calculated E value is 0.044 kJ/mol, which is very small compared to the 8 kJ/mol threshold, indicating that the adsorption process is mainly physical adsorption through van der Waals forces or electrostatic interactions. The Temkin model fit shows that the adsorption heat of CIP on ZnO decreases with increasing coverage of the ZnO surface. This may be due to the electrostatic repulsion between CIP molecules as they compete for adsorption sites on the ZnO surface. With the value of ΔH = 16.99 kJ/mol, which is in the average range, it suggests that adsorption may involve both physical and weak chemical mechanisms because $\Delta H < 20$ kJ/mol, the adsorption is mainly physical adsorption.

The influence of ZnO material mass on the ability to adsorb the CIP antibiotic is an important factor in

Table 5. Parameters of non-linear isotherms for CIP adsorption on ZnO nanoparticles.

Kinetic models	Equation	Parameters	Value
Langmuir	$q_e = \frac{q_m K_L C_e}{1 + K_L C_e}$ $R_L = \frac{1}{1 + K_L C_0}$	q_m (mg g^{-1})	298.89
		k_L (L mg^{-1})	0.0053
		R^2	0.9111
Freundlich	$q_e = K_F C_e^{1/n}$	1/n	0.7525
		k_F (mg g^{-1})/(mg L^{-1})$^{1/n}$	3.1551
		R^2	0.8839
Temkin	$q_e = B_T \ln K_T + B_T \ln C_e$	B_T	61.9958
		k_T (L mg^{-1})	0.0555
		R^2	0.9608
D-R	$q_e = q_m e^{-B\varepsilon^2}$	B (mol^2 (kJ^2)$^{-1}$	306.67
		q_m (mg g^{-1})	133.53
		R^2	0.9804

research on adsorbent materials. To study the effect of adsorbent dosage on CIP removal, 0.002–0.040 g L^{-1} of ZnO material was used to conduct adsorption experiments at an initial CIP concentration of 100 ppm, pH = 6, 90 min contact time and ambient temperature. According to the results in Fig. 7, when increasing the dose of ZnO from 0.005 to 0.04 g L^{-1}, the removal efficiency of CIP first increased from 72 to 80%, with the adsorption capacity gradually decreasing from 77.98 down to 13.88 mg g^{-1}. Similar adsorption trends were observed by Shang et al., who reported a significant increase in CIP removal efficiency from 36 to 100% when increasing the adsorbent dosage from 0.025 to 0.5 g L^{-1} [40]. The increase in CIP removal rate with increasing adsorption dose is due to the increase in available active sites, which enhances and increases CIP uptake [41]. When the volume of ZnO material is increased, the surface area available for interaction with CIP is also increased. Therefore, the adsorption capacity of ZnO material for CIP will be improved. Increasing the volume of material can result in faster and more efficient adsorption or removal of antibiotics from the solution. However, lead to volume of ZnO material can increase the saturation of the material, i.e., the maximum concentration of CIP that ZnO can adsorb before saturation. After reaching saturation, increasing the volume ZnO material no longer greatly affects the adsorption capacity.

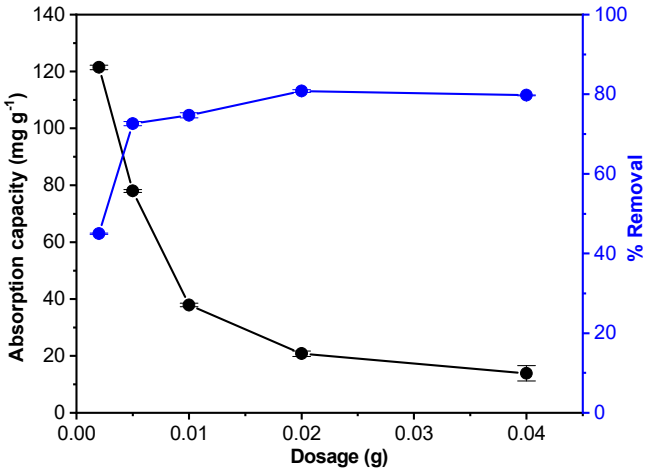

Fig 7. Effect of dose on CIP adsorption capacity on ZnO nanoparticles

The pH of the solution is an important parameter of the adsorption process because it affects the surface nature of the adsorbent and the adsorbent-adsorbate interaction. CIP is an antibiotic of the fluoroquinolone group [42]. CIP exists in three forms in solution: cationic form (with protonated amino group at pKa1 below 5.90), anionic form with deprotonated carboxylic acid group at pKa2 above 8.89. At pH between pKa1 and pKa2 of CIP, the CIP molecule exists in the zwitterionic form around pH 5.90 to 8.89. Fig. 8 shows the pH of the adsorption solution changes in the range of 1–10 during a contact time of 90 min, adsorption dose of 0.005 g L^{-1} and CIP antibiotic concentration of 100 ppm. The CIP

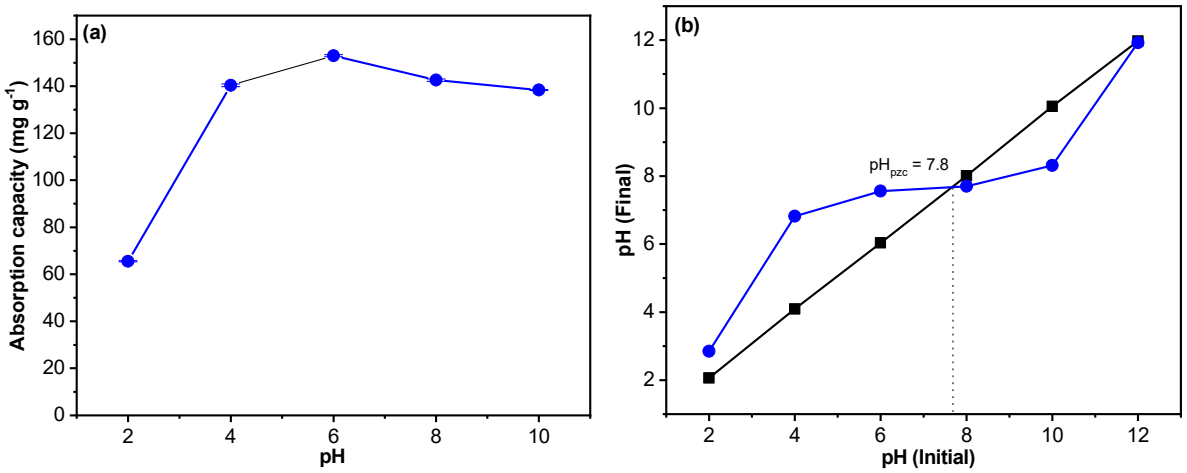

Fig 8. Effect of (a) pH and (b) pH_{pzc} on CIP adsorption capacity on ZnO nanoparticles

removal ability of ZnO increased with increasing solution pH from 2 to 6 and then decreased as the pH continued to increase. The pH_{pzc} is determined to be 7.8. This means that when the pH of the surrounding ZnO is lower than pH_{pzc}, the ZnO surface will have a positive charge. The negative carboxylate groups of CIP will be able to interact with the charge. Additionally, the highest CIP removal capacity was 152.93 mg g^{-1} at pH 6. At pH 6, the zwitter ion form of CIP reached the maximum percentage, facilitating the electrostatic attraction between the negatively charged atoms of the carboxyl group in CIP and the positively charged sites of the ZnO adsorbent surface [43].

Application Orientation for Skin Care Mask Products

SPF measures the effectiveness of protecting the skin from ultraviolet radiation. SPF is generally defined as the ratio of the amount of UV energy required to produce a minimum erythema dose (MED) on skin protected by a cosmetic product containing sunscreen to the amount of UV energy required to produce the same dose on unprotected skin. Using ZnO in facial mask formulations significantly contributes to the SPF and overall effectiveness of the facial mask product. Zinc oxide is an important ingredient known for its broad-spectrum UV protective properties, especially against UVB radiation (290–320 nm). The presence of ZnO in sunscreen formulations contributes significantly to the SPF value. SPF measures a product's effectiveness in protecting against UVB rays, and ZnO's ability to block UVB is shown in Table 6 and Fig. 9. Formula F0, without plant extracts, has the lowest SPF index of 6.15, while formulas F1-F5 have SPF values that vary according to the content of pennywort extract and the presence of ZnO, reaching the highest value. The highest SPF value is 14.12 in formula F4. Additionally, *C. asiatica* has skin-beneficial ingredients such as triterpenoids, flavonoids, and antioxidants that can protect the skin from the harmful effects of free radicals caused by sunlight, which can help

Table 6. SPF value and sun protection ability of the product

Formulation	SPF value	Sunlight resistance (%)
F0	6.15	83.75
F1	8.47	88.19
F2	11.80	91.53
F3	12.58	92.05
F4	14.12	93.92
F5	13.06	92.35

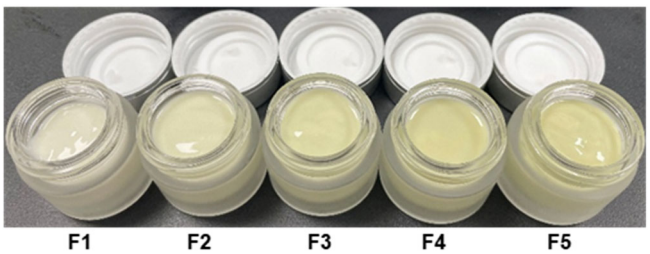

Fig 9. Skin care mask products change in different proportions

Table 7. SPF values of some products studied with sunscreen agents

Product	Material	SPF	Reference
Sunscreen cream	*Eucheuma cottonii* and *Kaempferia galanga*	16.7000	[44]
Sunscreen lotion	*Curcuma longa* L., *Aloe vera*, and *Alpinia galanga* Willd.	18.2010	[45]
Sunscreen cream	*Butea monosperma*	8.8727	[46]
Sunscreen cream	Tomato paste	21.0900	[47]
Sunscreen cream	*Glycyrrhiza glabra*, *Tinospora cordifolia*, and *Terminalia arjuna*	4.3700–24.2600	[48]

strengthen the skin. The product's SPF index is due to its antioxidant and skin-protecting properties.

When compared to other studies, the mask formula containing *C. asiatica* extract and ZnO showed an average SPF and moderate UV protection (Table 7). The current research formula has an average SPF, higher than some studies but lower than others. However, the formula has a strong competitive edge in the natural and gentle sunscreen cosmetics market due to its safe natural ingredients and skin-nourishing properties. *C. asiatica* extract is packed with polyphenols and flavonoids, which boost skin protection against UV rays and offer antioxidant, skin-soothing, and regeneration benefits. Additionally, ZnO is a broad-spectrum physical UV filter that is less irritating than chemical sunscreens. To enhance competitiveness, it is important to consider adjusting the ZnO ratio or incorporating other plant-based sunscreen compounds to increase SPF. Pairing with potent antioxidants like vitamins C and E can enhance skin protection efficacy. The focus should be developing safe natural products suitable for sensitive skin or daily use.

■ CONCLUSION

ZnO nanoparticles from pennywort extract is successfully synthesized with proven effective application activity. All modern analytical techniques, including UV-vis, XRD, FTIR, SEM imaging, and EDX analysis, demonstrated the successful synthesis of ZnO nanoparticles. The crystalline structure and hexagonal structure of the synthesized ZnO nanoparticles were determined by XRD study. The results depict that the CIP adsorption capacity is reduced at the operating condition for CIP adsorption on ZnO as pH 6, adsorption dose of 0.005 g L^{-1}, initial CIP concentration of 100 mg L^{-1}, and contact time of 90 min, yielded a significantly high CIP removal of 152.93 mg g^{-1}. The facial mask product also showed that it did not have any phase changes after being placed at room temperature for 1 week. Formula F4 has the highest SPF value among others, which is 14.12, by calculating absorbance using the Mansur equation. *C. asiatica* represents a promising natural source for green synthesis of ZnO nanoparticles tailored for cosmetic applications, providing a sustainable and biocompatible alternative to synthetic methods. Common nanoparticle compounds in the cosmetic industry. Therefore, it is necessary to conduct in-depth studies on the application of green synthetic ZnO materials in cosmetic formulations.

■ ACKNOWLEDGMENTS

This research is funded by Nguyen Tat Thanh University, Ho Chi Minh City, Vietnam under grant number 2024.01.07.

■ CONFLICT OF INTEREST

The authors have no conflict of interest.

■ AUTHOR CONTRIBUTIONS

Cat Thuyen Ngoc Vo and Cat Nguyen Ngoc Vo: conducted the experiment; Kim Ngan Thi Tran and Tuu Thi Tran: methodology and conducted the calculations; Khanh Van Tran Le: data curation; Kim Ngan Thi Tran and Hoang Danh Pham: writing - original draft, review & editing.

■ REFERENCES

[1] Hasnidawani, J.N., Azlina, H.N., Norita, H., Bonnia, N.N., Ratim, S., and Ali, E.S., 2016, Synthesis of ZnO nanostructures using sol-gel method, *Procedia Chem.*, 19, 211–216.

[2] Madathil, A.N.P., Vanaja, K.A., and Jayaraj, M.K., 2007, Synthesis of ZnO nanoparticles by hydrothermal method, *Proc. SPIE*, 6639, 66390J.

[3] Ghorbani, H.R., Mehr, F.P., Pazoki, H., and Rahmani, B.M., 2015, Synthesis of ZnO nanoparticles by precipitation method, *Orient. J. Chem.*, 31 (2), 1219–1221.

[4] Laurent, S., Forge, D., Port, M., Roch, A., Robic, C., Vander Elst, L., and Muller, R.N., 2008, Magnetic iron oxide nanoparticles: Synthesis, stabilization, vectorization, physicochemical characterizations, and biological applications, *Chem. Rev.*, 108 (6), 2064–2110.

[5] Agarwal, H., Venkat Kumar, S., and Rajeshkumar, S., 2017, A review on green synthesis of zinc oxide nanoparticles–An eco-friendly approach, *Resour.-Effic. Technol.*, 3 (4), 406–413.

[6] Upadhyaya, H., Shome, S., Sarma, R., Tewari, S., Bhattacharya, M.K., and Panda, S.K., 2018, Green synthesis, characterization and antibacterial activity of ZnO nanoparticles, *Am. J. Plant Sci.*, 9 (6), 1279–1291.

[7] Fakhari, S., Jamzad, M., and Kabiri Fard, H., 2019, Green synthesis of zinc oxide nanoparticles: A comparison, *Green Chem. Lett. Rev.*, 12 (1), 19–24.

[8] Mohammadi, C., Mahmud, S.A., Abdulla, S.M., and Mirzaei, Y., 2017, Green synthesis of ZnO nanoparticles using the aqueous extract of *Euphorbia petiolata* and study of its stability and antibacterial properties, *Morrocan J. Chem.*, 5 (3), 476–484.

[9] Akintelu, S.A., and Folorunso, A.S., 2020, A review on green synthesis of zinc oxide nanoparticles using plant extracts and its biomedical applications, *Bionanoscience*, 10 (4), 848–863.

[10] Nayak, S., Chaudhari, A., and Vaidhun, B., 2020, A review of zinc oxide nanoparticles: An evaluation of their synthesis, characterization and ameliorative properties for use in the food, pharmaceutical and cosmetic industries, *J. Excipients Food Chem.*, 11 (4), 2020.

[11] Sood, R., Darshitha, D., Mahesh, A.R., Rathore, S.S., and Jenita, J.L., 2023, Synthesis of zinc oxide nanoparticles using *Centella asiatica*, *Adv. Pharmacol. Pharm.*, 11 (4), 270–278.

[12] Jayachandran, A., Aswathy, T.R., and Nair, A.S., 2021, Green synthesis and characterization of zinc oxide nanoparticles using *Cayratia pedata* leaf extract, *Biochem. Biophys. Rep.*, 26, 100995.

[13] Soto-Robles, C.A., Luque, P.A., Gómez-Gutiérrez, C.M., Nava, O., Vilchis-Nestor, A.R., Lugo-Medina, E., Ranjithkumar, R., and Castro-Beltrán, A., 2019, Study on the effect of the concentration of *Hibiscus sabdariffa* extract on the green synthesis of ZnO nanoparticles, *Results Phys.*, 15, 102807.

[14] Darvishi, E., Kahrizi, D., and Arkan, E., 2019, Comparison of different properties of zinc oxide nanoparticles synthesized by the green (using *Juglans regia* L. leaf extract) and chemical methods, *J. Mol. Liq.*, 286, 110831.

[15] Rajini, K.P., Christie, C.A., Lisy, L., Alwin, T., and Sheeba, M.M., 2022, Green synthesis and characterization of zinc oxide nanoparticle using *Centella asiatica* leaf extract, *IJCRT*, 10 (2), 505–509.

[16] Doan Thi, T.U., Nguyen, T.T., Thi, Y.D., Ta Thi, K.H., Phan, B.T., and Pham, K.N., 2020, Green synthesis of ZnO nanoparticles using orange fruit peel extract for antibacterial activities, *RSC Adv.*, 10 (40), 23899–23907.

[17] Pavan Kumar, M.A., Suresh, D., and Sneharani, A.H., 2021, *Centella asiatica* mediated facile green synthesis of nano zinc oxide and its photo-catalytic and biological properties, *Inorg. Chem. Commun.*, 133, 108865.

[18] Sadiq, H., Sher, F., Sehar, S., Lima, E.C., Zhang, S., Iqbal, H.M.N., Zafar, F., and Nuhanović, M., 2021, Green synthesis of ZnO nanoparticles from *Syzygium cumini* leaves extract with robust photocatalysis applications, *J. Mol. Liq.*, 335, 116567.

[19] Altemimi, A., Lakhssassi, N., Baharlouei, A., Watson, D.G., and Lightfoot, D.A., 2017, Phytochemicals: Extraction, isolation, and identification of bioactive compounds from plant extracts, *Plants*, 6 (4), 42.

[20] Nobossé, P., Fombang, E.N., Singh, D., and Mbofung, C.M.F., 2021, Nanoencapsulation of antioxidant-rich fraction of roasted *Moringa oleifera* L. leaf extract: Physico-chemical properties and *in vitro* release mechanisms, *Food Nutr. Sci.*, 12 (9), 915–936.

[21] Mathavaraj, S., and Sabu, K.K., 2021, Genetic status of *Centella asiatica* (L.) Urb. (Indian pennywort): A review, *Curr. Bot.*, 12, 150–160.

[22] Belwal, T., Andola, H.C., Atanassova, M.S., Joshi, B., Suyal, R., Thakur, S., Bisht, A., Jantwal, A., Bhatt, I.D., and Rawal, R.S., 2019, "Gotu Kola (*Centella asiatica*)" in *Nonvitamin and Nonmineral Nutritional Supplements*, Eds. Nabavi, S.M., and Silva, A.S., Academic Press, Cambridge, MA, US, 265–275.

[23] Pham, H.N.T., Tang Nguyen, V., Van Vuong, Q., Bowyer, M.C., and Scarlett, C.J., 2017, Bioactive compound yield and antioxidant capacity of *Helicteres hirsuta* Lour. stem as affected by various solvents and drying methods, *J. Food Process. Preserv.*, 41 (1), e12879.

[24] Reis Mansur, M.C.P.P., Leitão, S.G., Cerqueira-Coutinho, C., Vermelho, A.B., Silva, R.S., Presgrave, O.A.F., Leitão, Á.A.C., Leitão, G.G., Ricci-Júnior, E., and Santos, E.P., 2016, *In vitro* and *in vivo* evaluation of efficacy and safety of photoprotective formulations containing antioxidant extracts, *Rev. Bras. Farmacogn.*, 26 (2), 251–258.

[25] Suresh, D., Nethravathi, P.C., Udayabhanu, U., Rajanaika, H., Nagabhushana, H., and Sharma, S.C., 2015, Green synthesis of multifunctional zinc oxide (ZnO) nanoparticles using *Cassia fistula* plant extract and their photodegradative, antioxidant and antibacterial activities, *Mater. Sci. Semicond. Process.*, 31, 446–454.

[26] Abdullah, J.A.A., Rosado, M.J., Guerrero, A., and Romero, A., 2023, Eco-friendly synthesis of ZnO-nanoparticles using *Phoenix dactylifera* L., polyphenols: Physicochemical, microstructural, and functional assessment, *New J. Chem.*, 47 (9), 4409–4417.

[27] Jiménez-Rosado, M., Gomez-Zavaglia, A., Guerrero, A., and Romero, A., 2022, Green synthesis of ZnO nanoparticles using polyphenol extracts from pepper waste (*Capsicum annuum*), *J. Cleaner Prod.*, 350, 131541.

[28] Gupta, M., Tomar, R.S., Kaushik, S., Mishra, R.K., and Sharma, D., 2018, Effective antimicrobial activity of green ZnO nano particles of *Catharanthus roseus*, *Front. Microbiol.*, 9, 2030.

[29] Zhao, L.H., Zhang, R., Zhang, J., and Sun, S.Q., 2012, Synthesis and characterization of biocompatible ZnO nanoparticles, *CrystEngComm*, 14 (3), 945–950.

[30] Zandi, S., Kameli, P., Salamati, H., Ahmadvand, H., and Hakimi, M., 2011, Microstructure and optical properties of ZnO nanoparticles prepared by a simple method, *Phys. B*, 406 (17), 3215–3218.

[31] Hasanpour, A., Niyaifar, M., Asan, M., and Amighian, J., 2013, Synthesis and characterization of Fe_3O_4 and ZnO nanocomposites by the sol–gel method, *J. Magn. Magn. Mater.*, 334, 41–44.

[32] Wahab, R., Ansari, S.G., Kim, Y.S., Seo, H.K., Kim, G.S., Khang, G., and Shin, H.S., 2007, Low temperature solution synthesis and characterization of ZnO nano-flowers, *Mater. Res. Bull.*, 42 (9), 1640–1648.

[33] Kołodziejczak-Radzimska, A., Markiewicz, E., and Jesionowski, T., 2012, Structural characterisation of ZnO particles obtained by the emulsion precipitation method, *J. Nanomater.*, 2012 (1), 656353.

[34] Khan, M., Ware, P., and Shimpi, N., 2021, Synthesis of ZnO nanoparticles using peels of *Passiflora foetida* and study of its activity as an efficient catalyst for the degradation of hazardous organic dye, *SN Appl. Sci.*, 3 (5), 1–17.

[35] Su, X., Zhao, X., Cui, C., Xi, N., Zhang, X.L., Liu, H., Yu, X., and Sang, Y., 2022, Influence of wurtzite ZnO morphology on piezophototronic effect in photocatalysis, *Catalysts*, 12 (9), 946.

[36] Chan, Y.Y., Pang, Y.L., Lim, S., and Chong, W.C., 2021, Facile green synthesis of ZnO nanoparticles using natural-based materials: Properties, mechanism, surface modification and application, *J. Environ. Chem. Eng.*, 9 (4), 105417.

[37] Yousefi, M., Gholami, M., Oskoei, V., Mohammadi, A.A., Baziar, M., and Esrafili, A., 2021, Comparison of LSSVM and RSM in simulating the removal of ciprofloxacin from aqueous solutions using magnetization of functionalized multi-walled carbon nanotubes: Process optimization using GA and

RSM techniques, *J. Environ. Chem. Eng.*, 9 (4), 105677.

[38] Wang, Y.X., Gupta, K., Li, J.R., Yuan, B., Yang, J.C.E., and Fu, M.L., 2018, Novel chalcogenide based magnetic adsorbent KMS-1/L-Cystein/Fe_3O_4 for the facile removal of ciprofloxacin from aqueous solution, *Colloids Surf., A*, 538, 378–386.

[39] El-Bendary, N., El-Etriby, H.K., and Mahanna, H., 2022, Reuse of adsorption residuals for enhancing removal of ciprofloxacin from wastewater, *Environ. Technol.*, 43 (28), 4438–4454.

[40] Shang, J.G., Kong, X.R., He, L.L., Li, W.H., and Liao, Q.J.H., 2016, Low-cost biochar derived from herbal residue: Characterization and application for ciprofloxacin adsorption, *Int. J. Environ. Sci. Technol.*, 13 (10), 2449–2458.

[41] Khoshnamvand, N., Ahmadi, S., and Mostafapour, F.K., 2017, Kinetic and isotherm studies on ciprofloxacin an adsorption using magnesium oxide nanopartices, *J. Appl. Pharm. Sci.*, 7 (11), 79–83.

[42] Sparkes, D., and Enoch, D.A., 2022, "Quinolones" in *Comprehensive Pharmacology*, Elsevier, Oxford, UK, 240–254.

[43] Srinivas, C., Ranjith Kumar, E., Tirupanyam, B.V, Singh Meena, S., Bhatt, P., Prajapat, C.L., Chandrasekhar Rao, T.V., and Sastry, D.L., 2020, Study of magnetic behavior in co-precipitated Ni–Zn ferrite nanoparticles and their potential use for gas sensor applications, *J. Magn. Magn. Mater.*, 502, 166534.

[44] Pratama, G., Yanuarti, R., Ilhamdy, A.F., and Suhana, M.P., 2019, Formulation of sunscreen cream from *Eucheuma cottonii* and *Kaempferia galanga* (Zingiberaceae), *IOP Conf. Ser.: Earth Environ. Sci.*, 278 (1), 012062.

[45] Rasheed, A., Shama, S.N., Mohanalakshmi, S., and Ravichandran, V., 2012, Formulation, characterization and *in vitro* evaluation of herbal sunscreen lotion, *Orient. Pharm. Exp. Med.*, 12 (4), 241–246.

[46] More, B.H., Sakharwade, S.N., Tembhurne, S.V., and Sakarkar, D.M., 2013, Evaluation of sunscreen activity of cream containing leaves extract of *Butea monosperma* for topical application, *Int. J. Res. Cosmet. Sci.*, 3 (1), 1–6.

[47] Sjahjadi, F.R., Febriyenti, F., and Lucida, H., 2022, Formula Optimization of a Sunscreen Cream of Tomato's Purified Extract, *Proceedings of the 2nd International Conference on Contemporary Science and Clinical Pharmacy 2021 (ICCSCP 2021)*, Atlantis Press, 42–48.

[48] Shah, Y., and Mewada, R., 2023, Preparation and evaluation of herbal sunscreen creams, *Int. J. Pharm. Chem. Anal.*, 10 (2), 116–124.